

# A Generalized Hybrid Method for Electromagnetic Scattering Analysis of Multiple Objects

Quang M. Nguyen\* and Ozlem Kilic

**Abstract**—We propose a generalized hybrid method to achieve time efficient and accurate solutions for electromagnetic scattering and radiation problems involving complex scenes with multiple objects. The method utilizes frequency domain solutions, and is based on dividing the original computational domain into smaller sub-domains. Each sub-domain is first solved independently, then the interactions between the sub-domains are accounted for through an iterative procedure. The main difference of the proposed hybrid method in comparison with the current hybrid methods or the domain decomposition methods available in the literature is that the proposed method allows users to have the freedom to choose from a variety of techniques for each sub-domain; such as integral equation (IE), analytical and asymptotic methods that suit the problem at hand best. Current hybrid or domain decompositions methods rely on a predetermined combination of numerical techniques. This flexibility in the choice of the method employed for each sub-domain in the generalized hybrid method is achieved by creating an interface capable of interacting between the different sub-domains properly. Furthermore, the method renders to parallel implementation as each sub-domain is solved independently. The hybrid method in its current state can be applied to two different scenarios: (i) multiple non-touching homogeneous objects, and (ii) inhomogeneous objects. Numerical examples of various combinations of IE, analytical and asymptotic methods are presented to validate the accuracy and the robustness of the generalized hybrid method.

## 1. INTRODUCTION

Full-wave methods, such as the method of moments (MoM) [1], finite different time/frequency domain (FDTD/FDFD) [2], or finite element method (FEM) [3,4] are the most accurate numerical methods for analyzing the interactions of electromagnetic fields with complex structures. However, they are inherently limited to moderately sized structures, because their computation costs (in terms of memory and CPU time) increase rapidly with the electrical size of the problem.

The past twenty years have witnessed various numerical techniques that were developed to reduce the overall time and memory requirements of full-wave techniques such as the fast multipole method (FMM) or its enhanced version, multilevel fast multipole algorithm (MLFMA), impedance matrix localization (IML), and adaptive integral method (AIM) [5–8]. However, when the problem size becomes too large to solve on conventional computers within a reasonable length of time, a divide-and-conquer strategy is the key to overcome this limitation.

The concept behind the proposed generalized hybrid method is similar to the domain decomposition methods (DDM) [9–12], which is also based on dividing the original computational domain into smaller sub-domains. However, unlike classical DDM, we do not formulate the interface between sub-domains in the form of matrix operators, which limit the choice of the solver for the sub-domain. The analytical solutions can't be incorporated in DDM since they are not in matrix form. Furthermore, the interface

---

*Received 14 February 2017, Accepted 28 April 2017, Scheduled 10 June 2017*

\* Corresponding author: Quang M. Nguyen (93nguyen@cua.edu).

The authors are with the Department of Electrical Engineering and Computer Science, The Catholic University of America, DC 20064, USA.

between sub-domains in DDM needs to be modified to incorporate different numerical solvers for individual sub-domains. This is understandable since different solvers have different matrix forms. In the proposed hybrid method, we create a general interface capable of interacting between the different numerical and analytical methods properly. The interactions between the sub-domains are predicted by an iterative approach.

Many researchers have been developing various hybrid methods that utilize combinations of different numerical techniques; such as MoM-FDTD, MoM-FEM, PO-MoM and so on [13–20]. However, these efforts typically require a fixed number of sub-domains, and the formulation is developed only for a specific combination of methods.

The generalized hybrid method overcomes these limitations by allowing the freedom to choose from a variety of available techniques, i.e., full-wave integral equation (IE), asymptotic or analytical methods, for any number of sub-domains. By having the ability to choose an appropriate method for each sub-domain, the user can reduce the complexity as well as the computational time for that sub-domain while still preserving the accuracy. For instance, analytical solutions can be chosen for canonical objects, while asymptotic approaches are preferable for electrically large objects. The preliminary results of the generalized hybrid method have been reported in our previous work [21–23].

The remainder of the paper will present the details of the generalized hybrid method as follows. In Section 2, we describe the generalized hybrid method in two different scenarios: (i) multiple non-touching homogeneous objects, and (ii) inhomogeneous objects. Section 3 is devoted for plane wave decomposition of electromagnetic fields, which is necessary in interfacing the various techniques available in the generalized hybrid method. Section 4 presents numerical examples of various combinations of methods to validate the accuracy and demonstrate the robustness of the proposed hybrid method. Finally, Section 5 provides conclusions.

## 2. THE GENERALIZED HYBRID METHOD

In this section, the generalized hybrid method is presented to demonstrate its ability to combine various numerical methods under one umbrella. This is achieved by dividing the original computational domain into smaller sub-domains. Each sub-domain is then solved independently using one of the most suitable methods for that domain, and finally the interactions between the sub-domains are accounted for through the interfacing between the sub-domains. By doing so, the total domain size can be reduced, which consequently decreases the memory requirements. Also, by providing the user the freedom to choose a suitable technique for each sub-domain, the computational time for that sub-domain can be reduced without any loss of accuracy as opposed to using a default full-wave numerical method, especially for electrically large structures. Furthermore, since each sub-domain can be solved for independently, the approach renders itself to parallel implementation, which would enable a faster solution. Two proposed generalized hybrid method is discussed in details in this section. The first approach is applied to multiple non-touching homogeneous objects, and the second approach is applied to inhomogeneous objects. Finally, the complexity and memory requirements for the hybrid method are investigated.

### 2.1. The Hybrid Method for Multiple Non-Touching Homogeneous Objects

The generalized hybrid method can handle multiple sub-domains as shown in Fig. 1. Each sub-domain can employ any suitable method available, such as MoM, Mie, physical optics (PO), equivalent dipole model (EDM), spherical wave expansion (SWE), etc. The choice of method is based on the specific properties of the sub-domain. For instance, if a sub-domain contains a canonical object, an appropriate analytical solution can be considered as the first priority. On the other hand, if a sub-domain contains an electrically large object of arbitrary shape, a suitable asymptotic approach such as PO may be preferred. And if the sub-domain contains a resonant size object, a full-wave numerical technique would be a good candidate. As shown in Fig. 2, the hybrid method first divides the original problem into a number of sub-domains; i.e.,  $N$  as depicted. The user then assigns an appropriate method to each sub-domain based on its properties. Then an iterative process begins where the fields for each sub-domain are solved for and updated by interactions between the sub-domains. The procedure stops when the relative change in all sub-domains is less than the user-defined criteria.

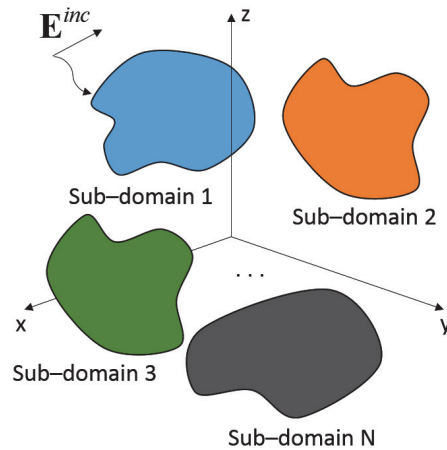


**Figure 1.** Scene with multiple non-touching homogeneous objects.

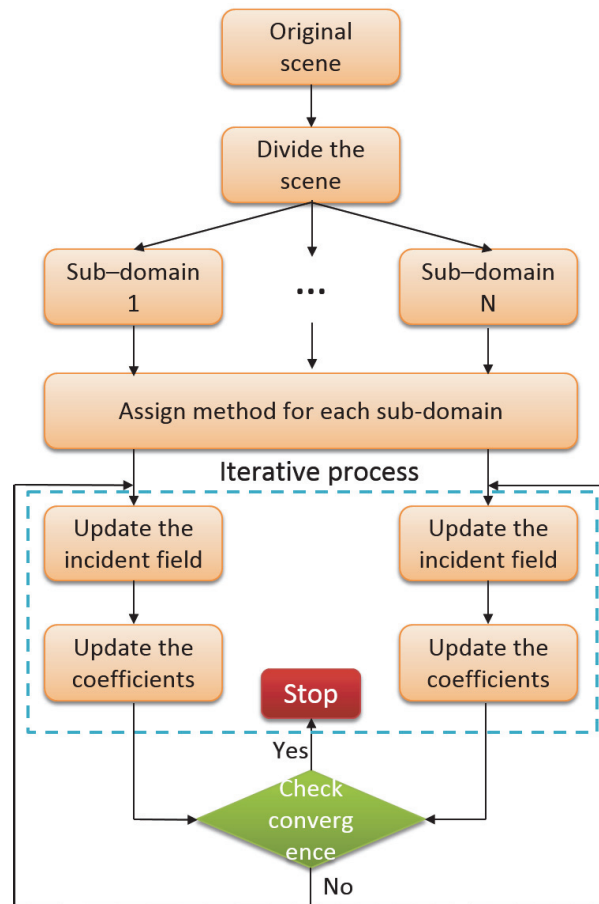


**Figure 2.** Block diagram of the generalized hybrid method for multiple non-touching homogeneous objects.

## 2.2. Iterative Procedure in the Hybrid Method for Multiple Non-Touching Homogenous Objects

At the time of the first iteration, the incident field on the scene,  $\mathbf{E}_{inc}$ , is assumed to be the only source of excitation. For the sake of simplicity, let's assume,  $N = 2$ , i.e., two sub-domains. Let's also assume

that MoM and Mie solutions are the methods of choice for sub-domain 1 and 2, respectively. It should be noted that the concept still holds if any other methods are applied to these sub-domains, and MoM and Mie are used only for demonstration purposes.

At the first iteration, the incident fields on the sub-domains equal the incident field on the scene.

$$\mathbf{E}_{inc(1)}^{(1)}(\mathbf{r}) = \mathbf{E}_{inc(2)}^{(1)}(\mathbf{r}) = \mathbf{E}_{inc}(\mathbf{r}). \quad (1)$$

where the subscript  $(i)$  is the sub-domain index; i.e.,  $i = 1, 2, \dots, N$ , and the superscript  $(j)$  refers to the index of iteration. Then we start the solution for sub-domain 1 using MoM by computing the induced currents on it, i.e.,  $\mathbf{J}_{(1)}^{(1)}(\mathbf{r})$ , due the incident field, i.e.,  $\mathbf{E}_{inc(1)}^{(1)}(\mathbf{r})$ . The electromagnetic fields radiated by this current; i.e.,  $\mathbf{e}_{rad(12)}^{(1)}(\mathbf{r})$ , are then calculated to illuminate sub-domain 2. Similarly, we start the solution for sub-domain 2 by analytically calculating (Mie) the radiated fields due to its illumination by  $\mathbf{E}_{inc(2)}^{(1)}(\mathbf{r})$ . Then these scattered fields; i.e.,  $\mathbf{e}_{rad(21)}^{(1)}(\mathbf{r})$ , are computed to illuminate sub-domain 1. The process for the first iteration is summarized in Fig. 3. It should be noted that in the subscript  $(ij)$ , the first index  $(i)$  denotes the original domain, and the second index  $(j)$  denotes the destination domain.

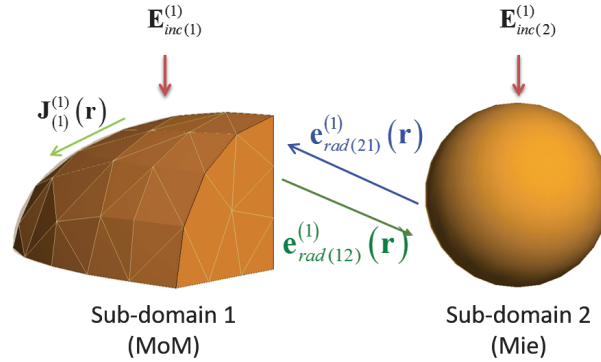


**Figure 3.** Generalized hybrid method - first iteration for multiple non-touching homogeneous objects.

For the second iteration, the fields for sub-domain 1 are equal to the sum of the original incident field and the radiated fields from sub-domain 2 to sub-domain 1 as shown in Eq. (2). Similarly, the fields for sub-domain 2 are equal to the sum of the original incident field and the radiated fields from sub-domain 1 to sub-domain 2 as in Eq. (3).

$$\mathbf{E}_{inc(1)}^{(2)}(\mathbf{r}) = \mathbf{e}_{rad(21)}^{(1)}(\mathbf{r}) + \mathbf{E}_{inc}(\mathbf{r}). \quad (2)$$

$$\mathbf{E}_{inc(2)}^{(2)}(\mathbf{r}) = \mathbf{e}_{rad(12)}^{(1)}(\mathbf{r}) + \mathbf{E}_{inc}(\mathbf{r}). \quad (3)$$

The iteration process between the sub-domains continues until the algorithm converges; i.e., the variation in terms of the induced current between the last two iterations,  $\gamma$ , is within a predetermined percentage. Finally, the total scattered field from the entire domain is calculated based on the sum of all scattered fields from the sub-domains at the final iteration.

The same concept is still applicable when the number of sub-domains is greater than two. The incoming field for any sub-domain is the summation of the original incident field and the radiated fields from all other sub-domains. The implementation is constructed so that the incoming field to each sub-domain is updated at the end of every iteration. The ordering of the sub-domains doesn't make a difference. This approach renders to a parallel implementation easily.

### 2.3. Interfacing the Sub-Domains for Multiple Non-Touching Homogenous Objects

The interface algorithm is dependent on the methods used for each-sub-domain pair. For the case of MoM-Mie as discussed above, the solution for sub-domain 1 (MoM) requires the knowledge of the total

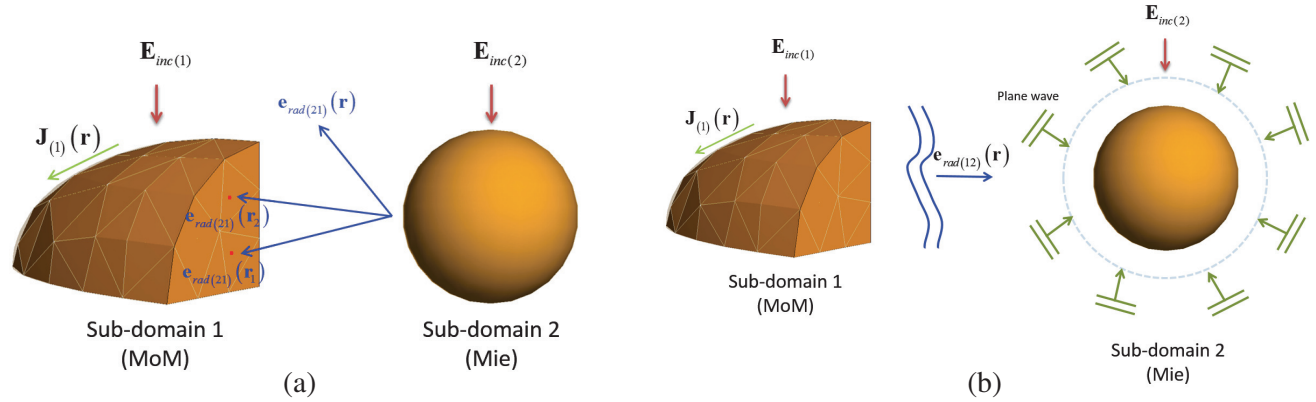


**Figure 4.** Interactions between the sub-domains for multiple non-touching homogeneous objects. (a) Sub-domain 2 to sub-domain 1. (b) Sub-domain 1 to sub-domain 2.

incident field at the center of each mesh element. Therefore, the radiated fields from sub-domain 2 to sub-domain 1, i.e.,  $\mathbf{e}_{rad(21)}(\mathbf{r})$  need to be evaluated at the center of each mesh element of sub-domain 1 as shown in Fig. 4(a). The solution for sub-domain 2 (Mie scattering) requires the incident field to be in the form of plane waves. Therefore, the radiated fields from sub-domain 1 to sub-domain 2,  $\mathbf{e}_{rad(12)}(\mathbf{r})$ , must be decomposed into plane waves illuminating sub-domain 2, as shown in Fig. 4(b). The details of decomposing the radiated field into plane waves will be discussed in Section 3.

In general, if the method on a sub-domain requires meshing, grid points, or sampling points, the incoming fields (from other sub-domains to that sub-domain) should be calculated at those special points. Similarly, if the method on that sub-domain requires the incident fields to be in the form of plane waves, the incoming fields from other sub-domains must be decomposed into a set of plane waves.

#### 2.4. The Generalized Hybrid Method for Inhomogeneous Objects

In this section, we present the hybrid method for inhomogeneous objects, as shown in Fig. 5. The block diagram of the algorithm is demonstrated in Fig. 6 for  $N$  sub-domains. The method employed in the exterior sub-domain, i.e., sub-domain 1, is MoM and the choice of methods for the interior sub-domains, i.e., sub-domains 2, 3,  $\dots$ ,  $N$  is based on the specific properties of these sub-domains.

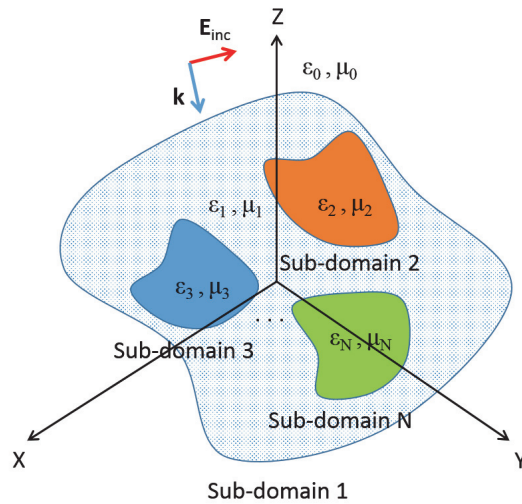


**Figure 5.** Scene with inhomogeneous objects.

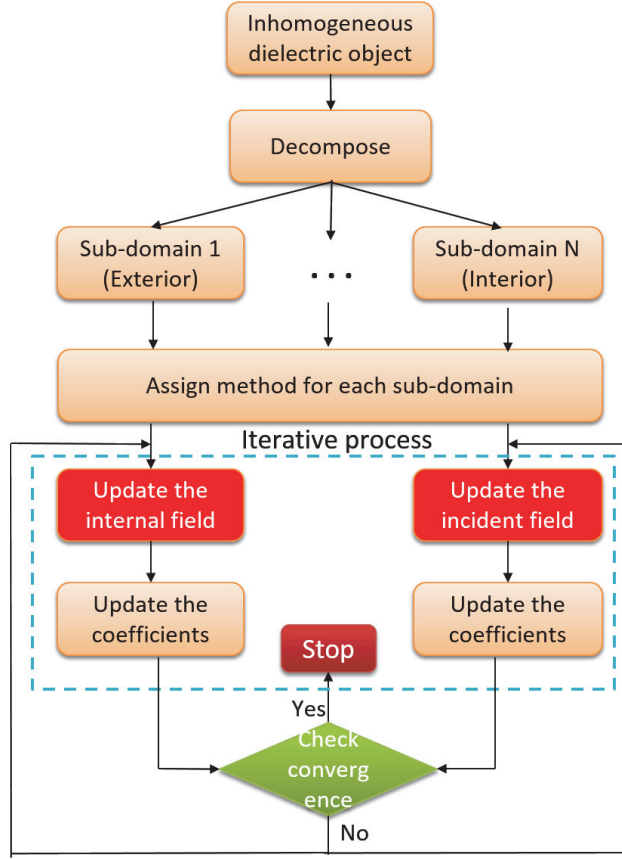


**Figure 6.** Block diagram of the generalized hybrid method for inhomogeneous objects.

#### 2.4.1. Iterative Procedure in the Hybrid Method for Inhomogeneous Objects

As shown in Fig. 5, a plane wave,  $\mathbf{E}_{inc}$ , illuminates the computational domain, and is assumed to be the only source of excitation at the time of the first iteration. For the sake of simplicity, let's assume  $N = 2$ , i.e., a two-layered dielectric object. Let's also assume that MoM is the method employed for both sub-domains. It should be noted that the concept can still be applied to the case of more complex inhomogeneous objects. The method employed in the exterior sub-domain, i.e., sub-domain 1, is MoM and the choice of method for the interior sub-domains, i.e., sub-domains  $2, 3, \dots, N$  is based on the specific properties of that sub-domain. If the interior sub-domains are touching, we can consider them as one sub-domain.

In the beginning, the inhomogeneous object is decomposed into two homogeneous domains, namely exterior domain (sub-domain 1) and interior domain (sub-domain 2) respectively, as shown in Fig. 7. At the first iteration, the field on the exterior domain (sub-domain 1) is equal to the incident field, as in (4), and the field on the interior domain (sub-domain 2) is 0, as in (5).

$$\mathbf{E}_{inc(1)}^{(1)}(\mathbf{r}) = \mathbf{E}_{inc}(\mathbf{r}), \quad (4)$$

$$\mathbf{E}_{inc(2)}^{(1)}(\mathbf{r}) = 0. \quad (5)$$

Then we start the solution for sub-domain 1 using MoM by computing the induced currents on it due to  $\mathbf{E}_{inc(1)}^{(1)}(\mathbf{r})$ . The internal fields generated by these currents,  $\mathbf{E}_{int(1)}^{(1)}(\mathbf{r})$  are then calculated to illuminate the interior domain (sub-domain 2) as shown in Eq. (6).

$$\mathbf{e}_{rad(12)}^{(1)}(\mathbf{r}) = \mathbf{E}_{int(1)}^{(1)}(\mathbf{r}). \quad (6)$$

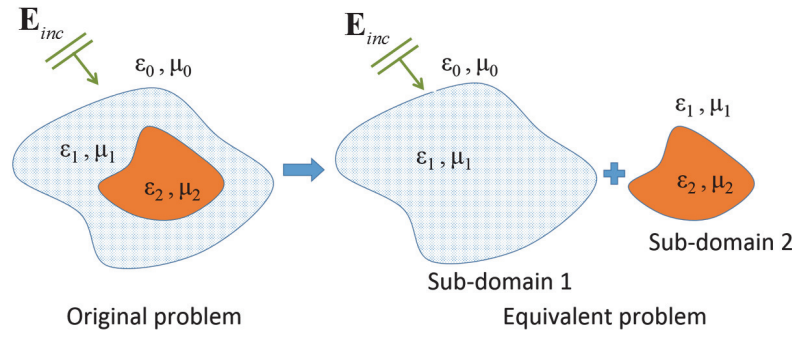


**Figure 7.** Decomposition of the inhomogeneous object.

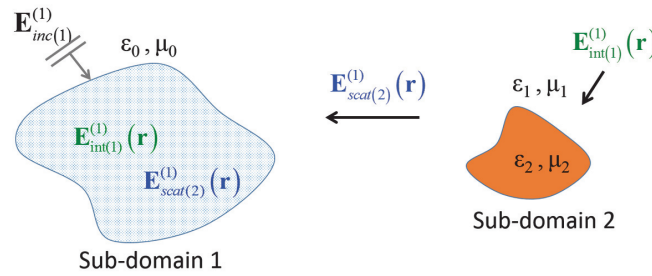


**Figure 8.** Generalized hybrid method — first iteration for inhomogeneous objects.

Sub-domain 2 receives these fields,  $\mathbf{e}_{rad(12)}^{(1)}(\mathbf{r})$ , as the incident fields,  $\mathbf{E}_{inc(2)}^{(1)}(\mathbf{r})$ , and then re-radiates them towards sub-domain 1 as shown in Eq. (7).

$$\mathbf{e}_{rad(21)}^{(1)}(\mathbf{r}) = \mathbf{E}_{scat(2)}^{(1)}(\mathbf{r}). \quad (7)$$

The process for the first iteration is summarized in Fig. 8.

For the second iteration, the total incident field for sub-domain 1 is the combination of the original plane wave,  $\mathbf{E}_{inc}$  and the radiated field,  $\mathbf{e}_{rad(21)}^{(1)}(\mathbf{r})$ , which was radiated from sub-domain 2 to 1. The incident field for domain 2 is then updated by  $\mathbf{e}_{rad(12)}^{(2)}(\mathbf{r})$  as shown in Eq. (8).

$$\mathbf{E}_{inc(2)}^{(2)}(\mathbf{r}) = \mathbf{e}_{rad(12)}^{(2)}(\mathbf{r}) = \mathbf{E}_{int(1)}^{(2)}(\mathbf{r}). \quad (8)$$

The iterative process continues until the algorithm converges, i.e., the variation in terms of the induced currents between the last two iterations,  $\gamma$ , is within a predetermined percentage. The internal fields and the radiated fields from sub-domains 1 and 2 are evaluated at the center of the mesh elements of sub-domains 2 and 1, respectively. If the solution of sub-domain 2 requires the incident field to be in the form of plane waves, the radiated fields from sub-domain 1 need to be decomposed into plane waves as discussed above.

#### 2.4.2. Interfacing the Sub-Domains for Inhomogeneous Objects

As discussed for the case of multiple non-touching objects, the updated total fields simply are the sum of the original incident field,  $\mathbf{E}_{inc}$ , and the radiated fields from other sub-domains. However, for the case of inhomogeneous objects, since the radiated fields from sub-domain 2 to 1,  $\mathbf{e}_{rad(21)}^{(1)}(\mathbf{r})$ , are considered as the internal fields of the sub-domain 1, as shown in Fig. 8, the updated total fields of the sub-domain 1 is the combination of the original incident field,  $\mathbf{E}_{inc}$  and the internal fields,  $\mathbf{E}_{scat(2)}^{(1)}(\mathbf{r})$ . Hence, when MoM is employed for sub-domain 1, the boundary condition must be modified by adding the new internal fields,  $\mathbf{E}_{scat(2)}^{(1)}(\mathbf{r})$ , to it. For the sub-domain 2, the updated incident fields are the internal fields calculated from sub-domain 1 to 2, as shown in Eq. (8).



## 2.5. Computational Complexity and Memory Requirements for the Hybrid Method

In this section, we investigate the complexity and memory requirements of the proposed hybrid method, and compare it to a full-wave solution, such as MoM. The computational resources required for the hybrid method depend on the choice of methods employed in the sub-domains.

We assume that the original problem decomposes into  $p$  sub-domains. If we employ MoM to solve the entire problem, (i.e., without decomposing it), the complexity and memory requirements of the problem would be  $O(N^3)$  and  $N^2$  respectively, where  $N$  is the total number of mesh elements in the original problem. For our proposed hybrid method with  $p$  sub-domains, the overall complexity would be the sum of the complexities of the sub-domain calculations and interfacing the sub-domains. The complexity of the sub-domain calculations would be determined by the worst case scenario; i.e., by accounting for the sub-domain that takes the longest computations, and can be expressed as  $N_{iter} \times \max\{O(N_1^3), O(N_2^3), \dots, O(N_p^3)\}$ , where  $N_{iter}$  is the number of iterations required for the hybrid method to converge, and  $N_i$  is the total number of mesh elements of the  $i$ th sub-domain. The complexity for interfacing the sub-domains depends on the complexity of calculating the radiated fields, which is approximately  $N$  for one observation point. For multiple observation points, the calculation of radiated fields can be constructed as a system of linear equations; i.e., where  $A$  is the matrix which represents the relationship between source points and observation points,  $x$  is the induced current, and  $B$  represents the radiated fields. The  $A$  matrix needs to be calculated only once for the first iteration, and can be reused for further iterations. Thus, the complexity of interfacing the sub-domains would be  $O(N^2)$ . Similarly, the memory requirements for the hybrid method would depend on the worst case scenario; i.e.,  $\max\{N_1^2, N_2^2, \dots, N_p^2\}$ , which will be, as expected, less than solving the problem without decomposing into sub-domains. It should be noted that an inherent benefit for the proposed hybrid method is that it renders to parallel computing as each sub-domain can be solved for independently before the interactions among them are computed. Furthermore, the calculation of radiated fields for different observation points also renders to parallel implementation since the currents in the mesh elements and the observation points are independent of each other.

Next, we use a simple example to analyze the complexity and memory requirements in the hybrid method. We assume that the original problem is decomposed into two sub-domains of the same size, and MoM is employed for both sub-domains. The complexity would be  $O(N_{iter} \frac{N^3}{8}) + O(\frac{N^2}{4})$  while the memory requirements are in the order of  $\frac{N^2}{4}$ . Thus, the hybrid method performs better than MoM in terms of computational time when  $N_{iter} < 8$ . Based on various numerical results, which will be discussed in Section 4, this is a likely scenario. The hybrid method only needs a few iterations to converge in the case of two sub-domains. Although the hybrid method may not gain much advantage compared to MoM in terms of computational time in the case of two sub-domains, it can save four times as much memory compared to MoM. Furthermore, each sub-domain can be solved in parallel to reduce computation time.

It is expected that as the number of sub-domains increase, the hybrid method would take longer to converge. To investigate the performance for problems with more than two sub-domains, and analyze the relationship between the number of iterations,  $N_{iter}$  and the number of sub-domains,  $p$  in the hybrid method, we devised a test case as shown in Fig. 9, where we added more sub-domains (spheres) to for each test case. Fig. 10 shows the relationship between the number of sub-domains and the number of iterations required to converge as the number of sub-domains is increased from 1 to 7. As we observe, the number of required iterations to converge increases rapidly with the number of sub-domains. We

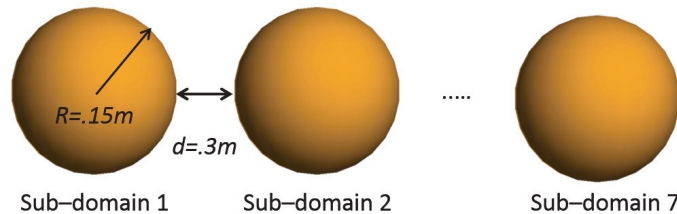
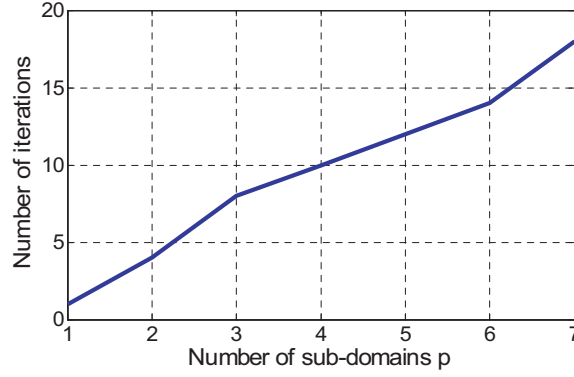


Figure 9. 7 spheres.





**Figure 10.** The number of iterations to converge,  $N_{iter}$  vs the number of sub-domains,  $p$ .

observe that for this test case when the number of sub-domains,  $p$ , is more than 3, the generalized hybrid method starts to slow down. However, the savings in memory requirements becomes more prevalent. The generalized hybrid method can save  $p^2$  times as much memory compared to MoM for the test case as shown in Fig. 9. Thus there is a tradeoff between the complexity and memory requirement in the generalized hybrid method. Although the scenario is selected for the case of multiple non-touching objects, similar results are found for the case of inhomogeneous objects.

### 3. THE PLANE WAVE DECOMPOSITION OF ELECTROMAGNETIC FIELDS

Many analytical solutions and numerical methods available for electromagnetics assume the incident field to be in the form of a plane wave. Hence, plane wave decomposition becomes an important issue for interfacing the sub-domains in the generalized hybrid method. By utilizing the spherical wave expansion, (SWE), we can decompose any arbitrary electromagnetic field into a set of plane waves. The suggested method involves three steps: (i) the electromagnetic fields are transformed into a series summation using SWE, (ii) SWE is converted to PWE, and (iii) the unknown SWE coefficients are obtained using a numerical technique.

Let us start by expressing the electromagnetic fields as an infinite series of discrete spherical waves as in [24]

$$\mathbf{E}(\mathbf{r}) = \sum_{n=1}^{\infty} \sum_{m=-n}^n Q_{mn}^{(1)} \mathbf{F}_{mn}^{(1)}(\mathbf{r}) + Q_{mn}^{(2)} \mathbf{F}_{mn}^{(2)}(\mathbf{r}), \quad r > r_0, \quad (9)$$

where  $Q_{mn}^{(i)}$  are the unknown expansion coefficients,  $\mathbf{F}_{mn}^{(i)}$  are the normalized spherical vector wave functions, and  $m, n$  are the indices of spherical order mode. The vector  $\mathbf{r}$  is the observation point, and  $r_0$  is the minimum radius of a sphere that contains the radiating object. The infinite summation in Eq. (9) is truncated at the finite index  $N$ , which is based on the relationship  $N \approx kr_0$ . Next, the spherical vector wave functions can be expanded into a sum of plane waves in the spectral  $\alpha\beta$ -domain as in [25] as:

$$\begin{aligned} \mathbf{F}_{mn}^{(1)}(\mathbf{r}) &= \frac{(-i)^{n+1}}{2\pi\sqrt{n(n+1)}} \int_{-\pi}^{\pi} \int_B \mathbf{Y}_{mn}(\alpha, \beta) e^{i\mathbf{k}\cdot\mathbf{r}} \sin(\alpha) d\alpha d\beta, \\ \mathbf{F}_{mn}^{(2)}(\mathbf{r}) &= \frac{(-i)^n}{2\pi\sqrt{n(n+1)}} \int_{-\pi}^{\pi} \int_B \left( \hat{\mathbf{k}} \times \mathbf{Y}_{mn}(\alpha, \beta) \right) e^{i\mathbf{k}\cdot\mathbf{r}} \sin(\alpha) d\alpha d\beta, \end{aligned} \quad (10)$$

where  $\beta$  is the spectral variable belonging to the interval  $[-\pi, \pi]$ ,  $\alpha$  is the spectral variable belonging to the complex contour  $B$ , as described in [26]. The unit vector  $\hat{\mathbf{k}}$  is defined as:

$$\hat{\mathbf{k}} = \mathbf{k}/k = \sin(\alpha) \cos(\beta) \hat{\mathbf{x}} + \sin(\alpha) \sin(\beta) \hat{\mathbf{y}} + \cos(\alpha) \hat{\mathbf{z}}. \quad (11)$$

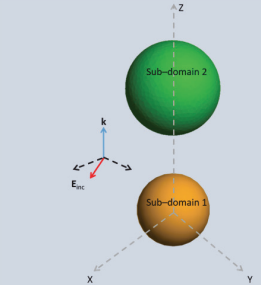
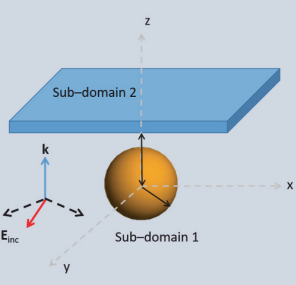
The real values of  $\alpha$  correspond to propagating waves, while the imaginary values correspond to evanescent waves. The terms  $\mathbf{F}_{mn}^{(1)}(\mathbf{r})$  and  $\mathbf{F}_{mn}^{(2)}(\mathbf{r})$  in Equation (10) are substituted in Equation (9) and the order of summation and integration is interchanged to obtain:

$$\mathbf{E}(\mathbf{r}) = \int_{-\pi}^{\pi} \int_B \left( \sum_{n=1}^{\infty} \sum_{m=-n}^n \frac{(-i)^{n+1}}{2\pi\sqrt{n(n+1)}} Q_{mn}^{(1)} \mathbf{Y}_{mn}(\alpha, \beta) + \frac{(-i)^n}{2\pi\sqrt{n(n+1)}} Q_{mn}^{(2)} (\hat{\mathbf{k}} \times \mathbf{Y}_{mn}(\alpha, \beta)) \right) \cdot e^{i\mathbf{k} \cdot \mathbf{r}} \sin(\alpha) d\alpha d\beta. \quad (12)$$

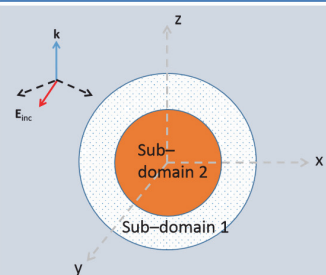
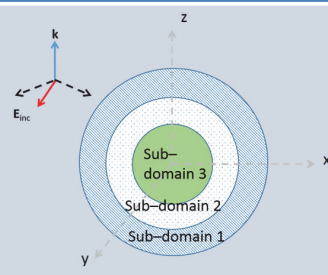
The integral in Equation (12) can be evaluated numerically by using a numerical technique such as the Gaussian quadrature [27,28]. Equation (12) enables us to express any electromagnetic field as a superposition of plane waves in the  $\alpha\beta$ -spectral domain. Finally, applying Fourier series technique can solve the unknown SWE coefficients. The more details of plane wave decomposition method can be found in [29].

#### 4. NUMERICAL RESULTS

This section demonstrates the ability of combining various techniques without modifying the formulation in the generalized hybrid method. Several examples are presented to validate the accuracy, as shown in Fig. 11 and Fig. 12. Scenario 1, as depicted in Fig. 12, considers two specific cases for multiple non-touching homogeneous objects: (i) one PEC sphere and one dielectric sphere, and (ii) a finite wall and a PEC sphere. Scenario 2 includes two test cases, as shown in Fig. 12: (i) a two-layered dielectric sphere, (ii) a three-layered dielectric sphere.

| Scenario 1 | Test case 1   |         | Test case 2  |        |
|------------|---|---------|--|--------|
| Model      |  |         |  |        |
| Methods    | MoM-MoM   | MoM-Mie | SWE-PO   | EDM-PO |

**Figure 11.** Test cases for multiple non-touching homogeneous objects.

| Scenario 2 | Test case 1   |         | Test case 2  |
|------------|---|---------|--|
| Model      |  |         |  |
| Methods    | MoM-SWE   | MoM-EDM | MoM-MoM-MoM  |

**Figure 12.** Test cases for inhomogeneous objects.

We will investigate each scenario by employing two different combinations of methods to solve for all test cases. We will also investigate the effects of different error margins for each method: i.e.,  $\gamma < 5\%$  and  $\gamma < 10\%$ . For all test cases in both scenarios, the scene is excited by a  $45^\circ$ -polarized plane wave operating at 1 GHz and propagating along the  $z$  direction. The results of the generalized hybrid method, and comparisons for different methods and error margins are provided in the following sub-sections. All results will be run using a personal computer (Intel Core i7 @ 1.7 GHz, 8 GB RAM) and will be compared to the commercial software package FEKO.

#### 4.1. Scenario 1 — Multiple Non-Touching Homogeneous Objects

Two test cases are considered in Scenario 1 to demonstrate its applicability to scenes with different features. We aim to demonstrate suitable methods and their applicability for objects of various size and nature. For the first test case, the problem is chosen so that one sub-domain contains an electrically small object (sub-domain 1), and the other sub-domain contains a canonical object (sub-domain 2). Fig. 13 shows the configuration for the first case. Full-wave methods (i.e., MoM) and the analytical solutions (i.e., Mie) are good candidates for the sub-domains in this scenario. Thus, we will study two methods: (i) MoM-MoM, and (ii) MoM-Mie, where the first method (MoM in both cases) is associated with sub-domain 1, and the second method (MoM or Mie) refers to sub-domain 2.

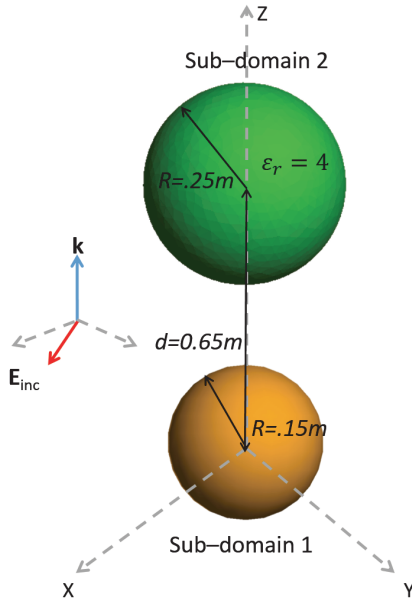


**Figure 13.** Test Case 1: One PEC sphere and one dielectric sphere.

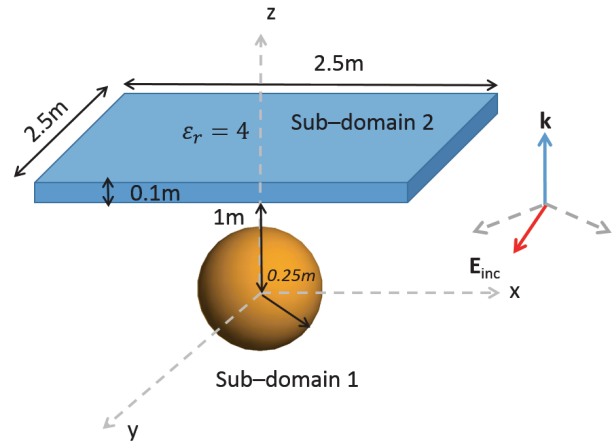


**Figure 14.** Test Case 2: A finite wall ( $2.5 \times 2.5 \times 0.1$  m,  $\varepsilon_r = 4$ ) and a sphere ( $r = 0.25$  m).

For the second test case, we have a PEC sphere (sub-domain 1) and an electrically large object of arbitrary shape (sub-domain 2). The configuration of the second test case is shown in Fig. 14. An asymptotic approach (i.e., PO) is suitable for the large object. Since we already investigated the applicability of the full wave method for the PEC sphere in test case 1, for this test case as an alternative, we employ generalized multipole techniques (i.e., SWE, EDM) for the small PEC sphere. Hence, we will study two methods for this test case: (i) SWE-PO, and (ii) EDM-PO.

##### 4.1.1. Iterative Results for Test Case 1: One PEC Sphere and One Dielectric Sphere

For the first test case, sub-domain 1 consists of the PEC sphere with radius of 0.15 m ( $\lambda/2$ ) and sub-domain 2 consists the dielectric sphere ( $\varepsilon_r = 4$ ) with radius of 0.25 m ( $\approx 0.83\lambda$ ). They are separated by a distance,  $d = 0.65$  m, along the  $z$  direction as shown in Fig. 13. We consider two methods, i.e., MoM-MoM and MoM-Mie, as described before. For the first method (MoM-MoM), both sub-domains employ

the full-wave method (MoM). The mesh size is  $\lambda/10$ , corresponding to approximately 900 unknowns for the smaller PEC sphere, and 2.3K unknowns for the dielectric sphere.

For the second method (MoM-Mie), we employ MoM for the first sub-domain (mesh size:  $\lambda/10$ ,  $N_{mesh} \approx 900$ ) and we employ the Mie solution for sub-domain 2. In this case we need to apply the PWE procedure, described in Section 3 to interface MoM with Mie solution. We use  $M = 800$  for the plane waves in the PWE step. It should be noted that the number of plane waves will be proportional to object's size and  $M = 800$  is a good choice for a sphere with  $r = 0.25$  m at 1 GHz regarding to the accuracy and processing time.

We show the results for the backscattered fields on a half circle ( $R = 1$  m from the origin) on the  $x$ - $z$  plane for both methods in Fig. 15 for the error,  $\gamma < 5\%$ , and in Fig. 16 for  $\gamma < 10\%$ . The red solid line and the dashed blue line show the fields calculated using the two hybrid methods, i.e., MoM-MoM, and MoM-Mie respectively. The dotted green line shows the fields obtained from the commercial software package FEKO. We observe that both hybrid methods offer a good agreement with FEKO.

The performance of the hybrid methods for this test case is shown in Table 1. As we can see, for MoM-MoM combination, the generalized hybrid method converges after 4 iterations and 125 seconds for  $\gamma < 5\%$ , and 3 iterations and 110 seconds for  $\gamma < 10\%$ . The total number of unknowns is roughly 2.3K. FEKO took 110seconds to solve the same problem with the same total number of unknowns.

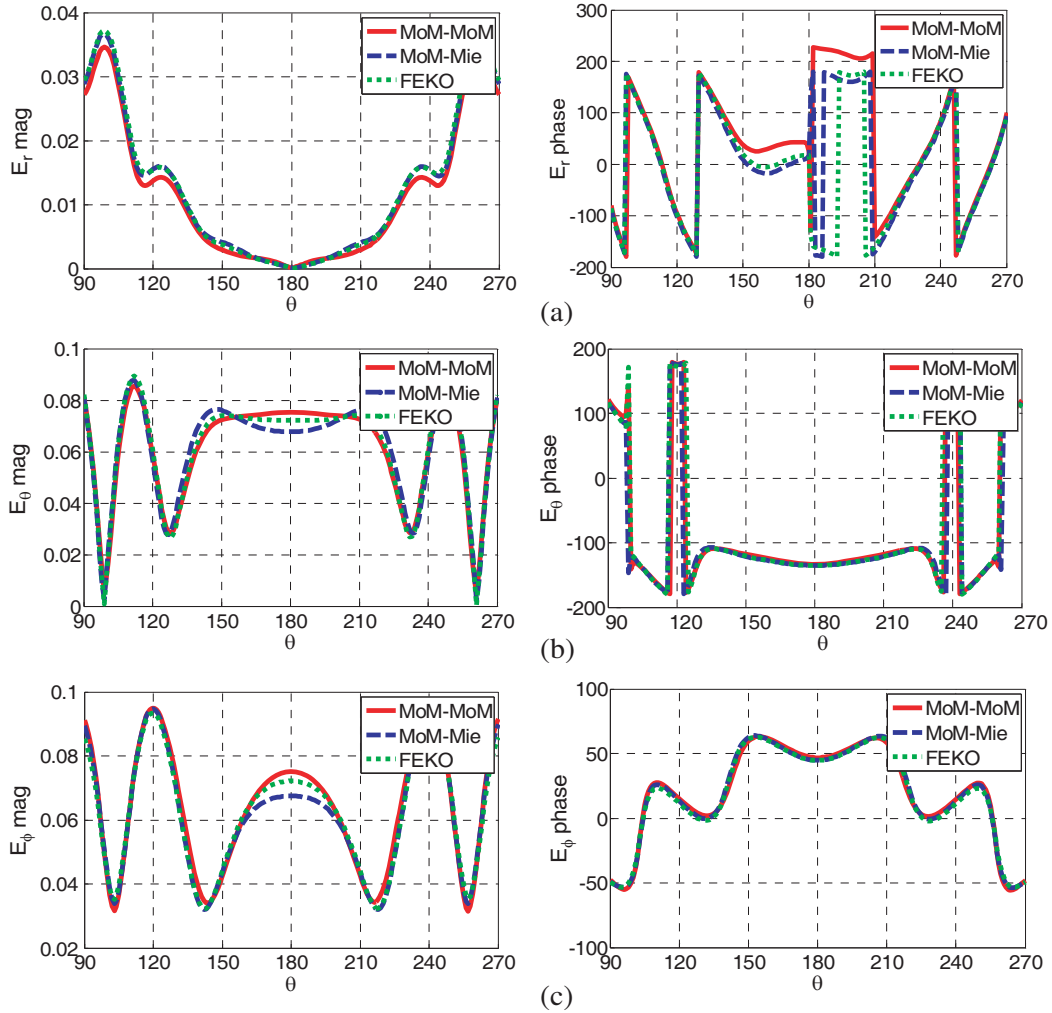


**Figure 15.** Backscattered field of one PEC sphere and one dielectric at  $f = 1$  GHz using MoM-MoM and MoM-Mie for  $\gamma < 5\%$ . (a)  $E_r$  component magnitude and phase. (b)  $E_\theta$  component magnitude and phase. (c)  $E_\phi$  component magnitude and phase.

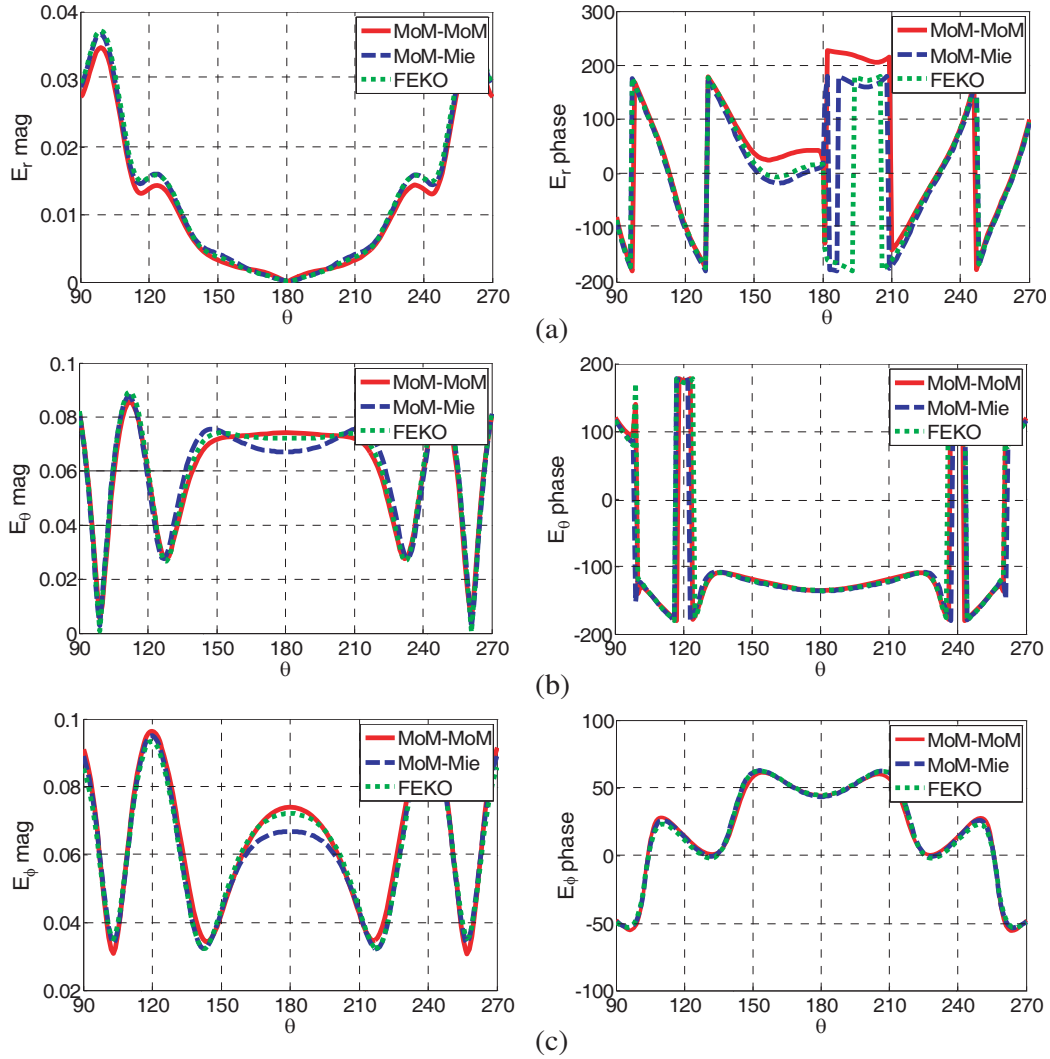


**Figure 16.** Backscattered field of one PEC sphere and one dielectric at  $f = 1$  GHz using MoM-MoM and MoM-Mie for  $\gamma < 10\%$ . (a)  $E_r$  component magnitude and phase. (b)  $E_\theta$  component magnitude and phase. (c)  $E_\phi$  component magnitude and phase.

**Table 1.** Performance of the hybrid method for scenario 1, test case 1.

| Methods              | MoM-MoM        |                 | MoM-Mie        |                 |
|----------------------|----------------|-----------------|----------------|-----------------|
| # Unknowns (Maximum) | $\sim 2.3$ K   |                 | $\sim 900$     |                 |
| # Iterations         | $\gamma < 5\%$ | $\gamma < 10\%$ | $\gamma < 5\%$ | $\gamma < 10\%$ |
|                      | 4              | 3               | 4              | 3               |
| Time                 | 125 s          | 110 s           | 60 s           | 50 s            |

In this test case, sub-domain 2 is much larger than sub-domain 1 ( $\sim 2.3$  K unknowns vs.  $\sim 900$  unknowns), and it consumes most of the time in the hybrid method. Thus, the performance of the hybrid method is slower than that of FEKO due to the required iterations to interface the sub-domains. Dividing the domain into two sub-domains and still using MOM for both cases would not necessarily be the best approach for this case. We would like to demonstrate the advantage of being able to choose a suitable approach with this test case, as we demonstrate below by using a better choice for sub-domain 2.

For the second method, we employ Mie scattering for the larger sphere (sub-domain 2), which helps improve the performance of the hybrid method. It should be noted that the PWE needed to interface the two methods renders to reduced computation time since one only needs to scale the amplitudes and phases of the  $M$  plane waves incident on sub-domain 2. Thus, the scattered fields from sub domain 2 need to be calculated only once at the first iteration. Furthermore, each plane wave is independent so the analytical method can be parallelized. These properties provide considerable relief in the computation time since the analytical method needs to be called only once during the entire process. With the choice of MoM-Mie for this test case, the generalized hybrid method took 4 iterations and 60 seconds for  $\gamma < 5\%$ , and 3 iterations and 50 seconds for  $\gamma < 10\%$  offering a speed up factor of 2 compared to FEKO.

#### 4.1.2. Results for Test Case 2: A Finite Dielectric Wall and PEC Sphere

For the second test case, sub-domain 1 consists of a PEC sphere with radius of 0.25 m ( $\approx 0.83\lambda$ ), and sub-domain 2 consists of a dielectric wall ( $\varepsilon_r = 4$ ) with dimensions,  $2.5 \times 2.5 \times 0.1$  m ( $\approx 8.3\lambda \times 8.3\lambda \times 0.33\lambda$ ). The dielectric wall resides on the  $x$ - $y$  plane, positioned at  $z = 1$  m as shown in Fig. 14.

We consider two methods, i.e., SWE-PO and EDM-PO. In both methods, we need to apply the

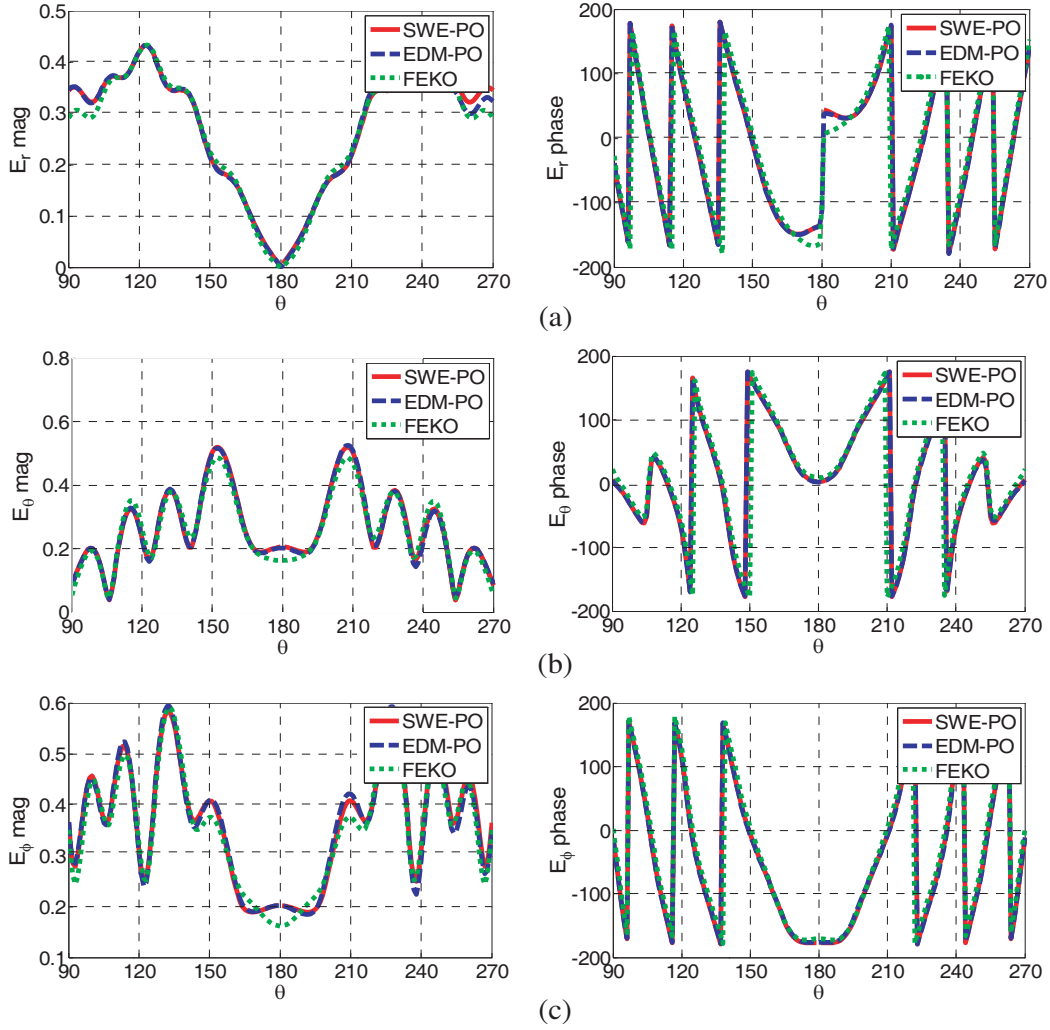


**Figure 17.** Backscattered field of a finite wall and a sphere at  $f = 1$  GHz using SWE-PO and EDM-PO for  $\gamma < 5\%$ . (a)  $E_r$  component magnitude and phase. (b)  $E_\theta$  component magnitude and phase. (c)  $E_\phi$  component magnitude and phase.



PWE procedure. We employ  $M = 800$  for the plane waves in the PWE step. For the first method (SWE-PO), we employ SWE for sub-domain 1 (PEC sphere) and PO for sub-domain 2 (finite dielectric wall). The number of spherical modes is  $N = 10$  for the SWE. For the second method (EDM-PO), EDM is employed for the sub-domain 1 and PO is employed for the sub-domain 2. The surface of the sphere is discretized uniformly by choosing  $M = 961$  points, and the number of dipoles is chosen as  $N = 225$ .

The total backscattered field from the scene on the  $x$ - $z$  plane is shown in Fig. 17 for  $\gamma < 5\%$  and Fig. 18 for  $\gamma < 10\%$ . The red solid and dashed blue lines show the results of both hybrid methods. The dotted green line shows the fields obtained from FEKO. We observe that both hybrid methods show good agreement with FEKO. The performance of the hybrid methods for this test case is shown in Table 2. As we can see, for SWE-PO combination, the generalized hybrid method converges after 5 iterations and 150 seconds for  $\gamma < 5\%$ , and 3 iterations and 100 seconds for  $\gamma < 10\%$ . It should be noted that, the PO method needs to be called only once during the entire process as discussed above. The total number of unknowns is roughly 21 K. FEKO took approximately 24 hours to solve the entire problem since the number of unknowns exceeds the memory for in-core solver.

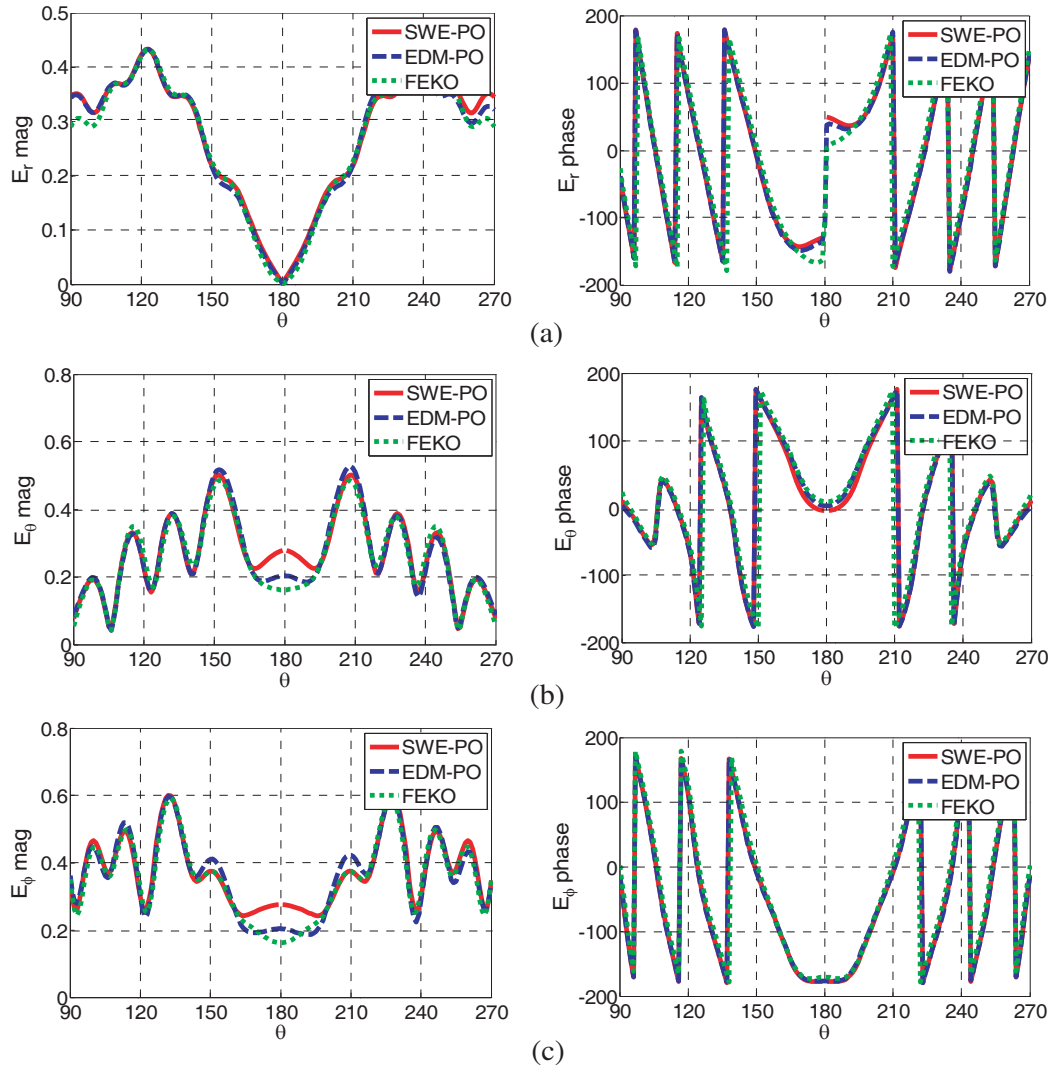


**Figure 18.** Backscattered field of a finite wall and a sphere at  $f = 1$  GHz using SWE-PO and EDM-PO for  $\gamma < 10\%$ . (a)  $E_r$  component magnitude and phase. (b)  $E_\theta$  component magnitude and phase. (c)  $E_\phi$  component magnitude and phase.



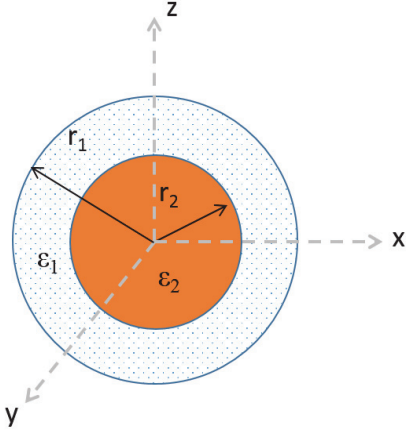
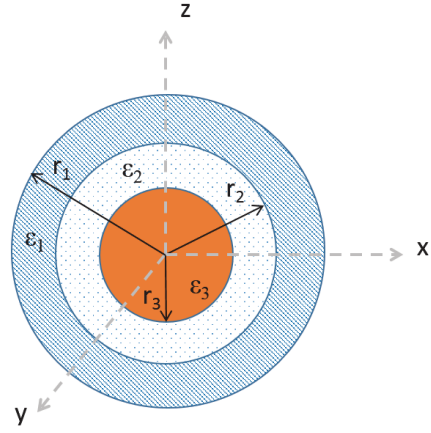
**Table 2.** Performance of the hybrid methods for scenario 1, test case 2.

| Methods              | SWE-PO         |                 | EDM-PO         |                 |
|----------------------|----------------|-----------------|----------------|-----------------|
| # Unknowns (Maximum) | $\sim 500$     |                 | $\sim 500$     |                 |
| # Iterations         | $\gamma < 5\%$ | $\gamma < 10\%$ | $\gamma < 5\%$ | $\gamma < 10\%$ |
|                      | 5              | 3               | 5              | 3               |
| Time                 | 150 s          | 100 s           | 400 s          | 250 s           |

For the second method, EDM-PO, the generalized hybrid method converges after 5 iterations and 400 seconds for  $\gamma < 5\%$ , and 3 iterations and 250 seconds for  $\gamma < 10\%$ . As we can see, EDM-PO combination is slower than SWE-PO combination. It is due to the number of dipoles required in EDM are larger than the number of spherical mode in SWE.

#### 4.2. Scenario 2 — Inhomogeneous Objects

Two test cases are considered in this scenario. The first test case consists of a two-layered dielectric sphere. The configuration of the first test case is shown in Fig. 19. In this test case, we present two methods; MoM-SWE, and MoM-EDM where sub-domain 1 (interior sphere) employs MoM, and sub-domain 2 (exterior sphere) employs either SWE or EDM. For the second test case includes a three-layered dielectric sphere. The configuration of the second test case is shown in Fig. 20. In this test case, we employ MoM in all sub-domains.

**Figure 19.** Geometry of test case 1 with a two-layered sphere ( $r_1 = 0.3$  m,  $r_2 = 0.2$  m).**Figure 20.** Geometry of test case 2 with a three-layered sphere ( $r_1 = 0.3$  m,  $r_2 = 0.2$  m,  $r_3 = 0.1$  m).

##### 4.2.1. Results for Test Case 1: A Two-Layered Sphere

For the first test case, sub-domain 1 consists the exterior sphere with a radius of 0.3 m ( $\lambda$ ) and sub-domain 2 consists of the interior sphere with a radius of 0.2 m ( $\approx 0.67\lambda$ ). The interior sphere will be considered PEC and the exterior sphere has a permittivity of  $\epsilon_r = 2$ . For the first method (MoM-SWE), we employ MoM for the first sub-domain and SWE for the sub-domain 2. The mesh size is  $\lambda/8$ , corresponding to approximately 2.2 K unknowns for the MoM. The number of spherical modes is  $N = 10$  for the SWE. For the second method (MoM-EDM), we employ MoM for the first sub-domain (mesh size:  $\lambda/8$ ,  $N_{mesh} \approx 2.2$  K) and EDM for the sub-domain 2. The surface of the sphere is discretized uniformly by choosing  $M = 961$  points, and the number of dipoles is chosen as  $N = 225$ .

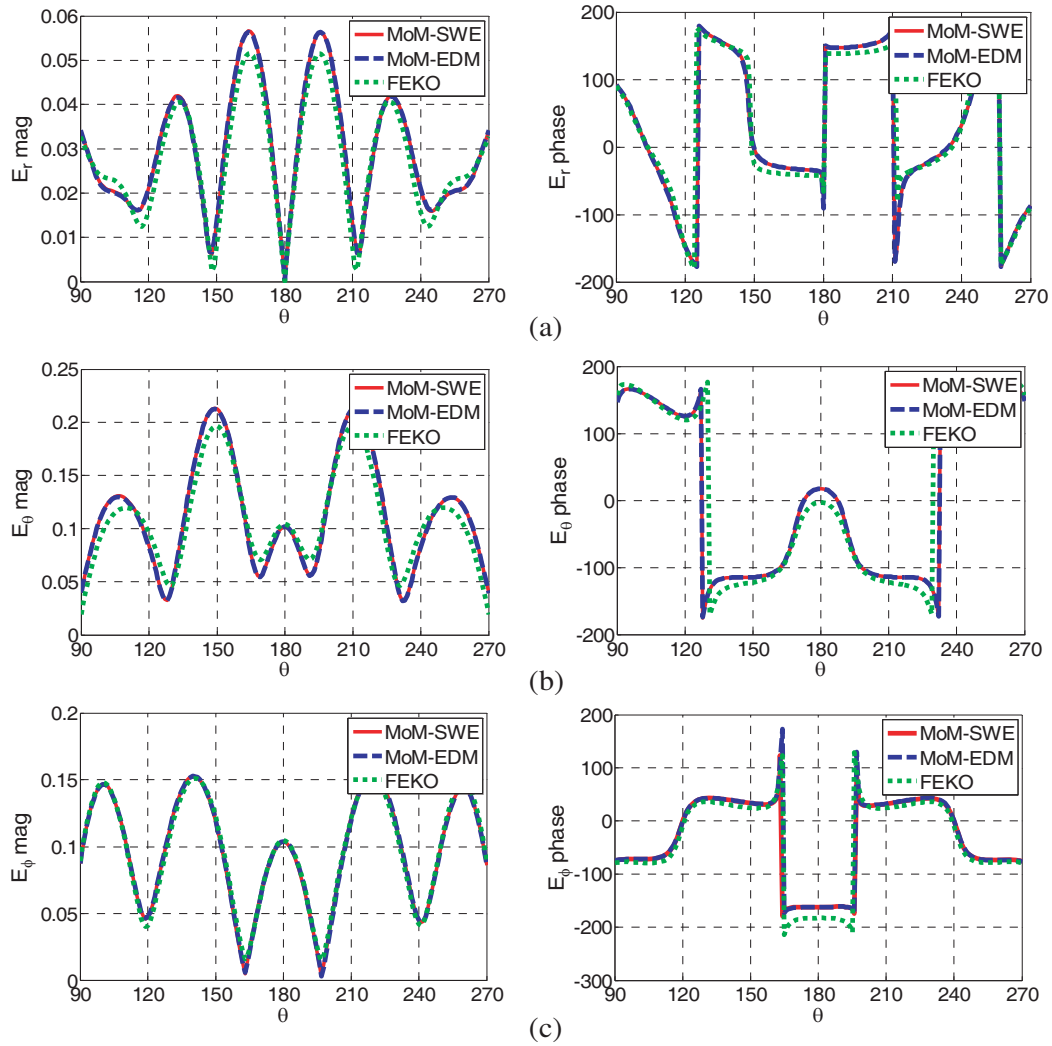


**Figure 21.** Backscattered field of test case 1 with a two-layered sphere using MoM-SWE and MoM-EDM for  $\gamma < 5\%$ . (a)  $E_r$  component magnitude and phase. (b)  $E_\theta$  component magnitude and phase. (c)  $E_\phi$  component magnitude and phase.

We show the results for the backscattered fields on a half circle ( $R = 1$  m from the origin) on the  $x$ - $z$  plane for both methods in Fig. 21 and Fig. 22 for  $\gamma < 5\%$  and  $\gamma < 10\%$ . The red solid line and dashed blue line show the fields calculated using the two hybrid methods, i.e., MoM-SWE, and MoM-EDM respectively. The dotted green line shows the fields obtained from the commercial software package FEKO. We observe that both hybrid methods show a good agreement with FEKO. The performance of the hybrid methods for this test case is shown in Table 3. As we see, for both combination, i.e., MoM-SWE, and MoM-EDM, the generalized hybrid method converges after 7 iterations and 142 seconds for  $\gamma < 5\%$ , and 6 iterations and 123 seconds for  $\gamma < 10\%$ . The total number of unknowns is roughly 3.1 K. FEKO took 125 seconds to solve the same problem with the same total number of unknowns. Thus, both methods can help save memory while their performances are comparable to FEKO.

#### 4.2.2. Results for Test Case 2: A Three-Layered Dielectric Sphere

For the second test case, the problem is decomposed into three sub-domains such that the first sub-domain corresponds to the exterior sphere ( $r_1 = 0.3$  m,  $\varepsilon_1 = 2$ ), the second sub-domain corresponds to the middle-layer sphere ( $r_2 = 0.2$  m,  $\varepsilon_2 = 4$ ), and the third sub-domain corresponds to the interior

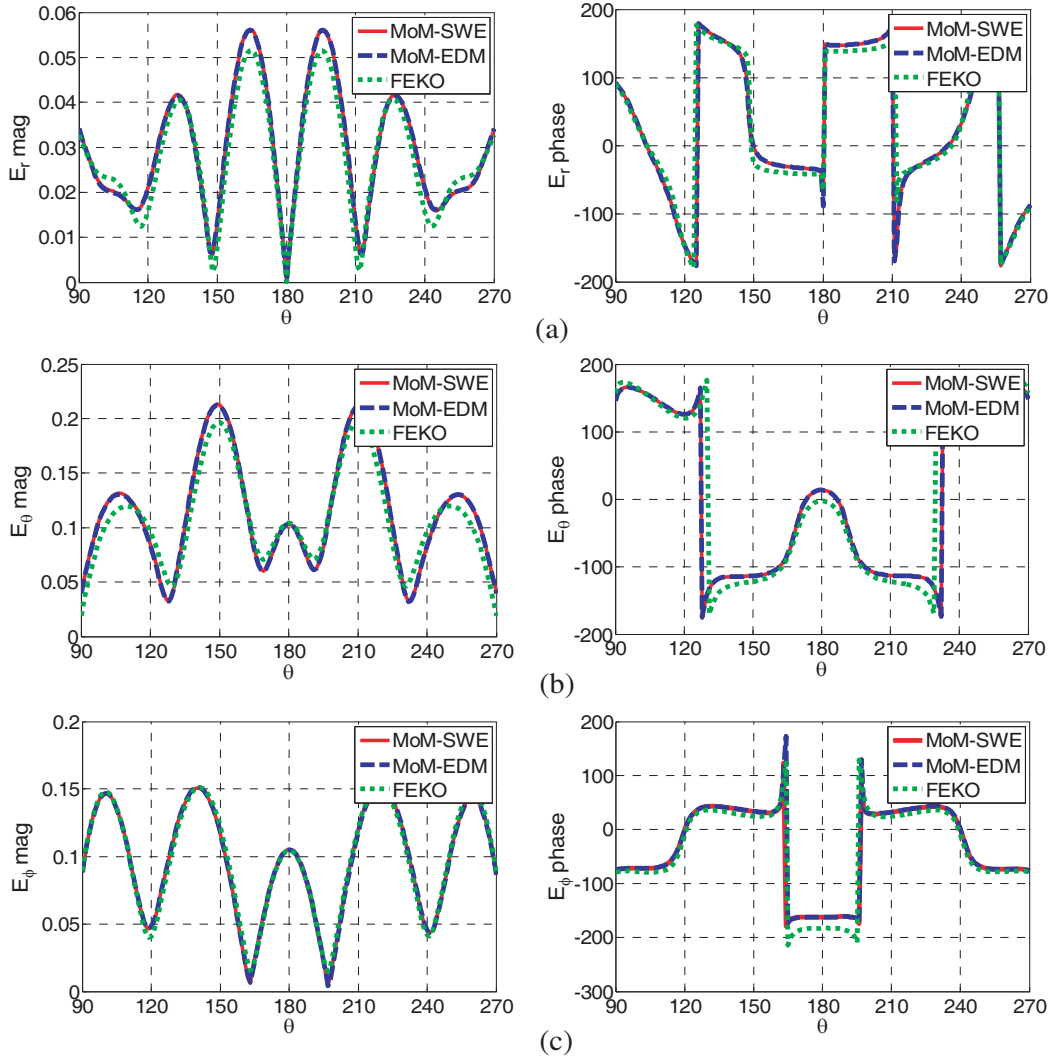


**Figure 22.** Backscattered field of a two-layered sphere at  $f = 1$  GHz using MoM-SWE and MoM-EDM for  $\gamma < 10\%$ . (a)  $E_r$  component magnitude and phase. (b)  $E_\theta$  component magnitude and phase. (c)  $E_\phi$  component magnitude and phase.

**Table 3.** Performance of the hybrid methods for scenario 2, test case 1.

| Methods              | MoM-SWE        |                 | MoM-EDM        |                 |
|----------------------|----------------|-----------------|----------------|-----------------|
| # Unknowns (Maximum) | $\sim 2.2$ K   |                 | $\sim 2.2$ K   |                 |
| # Iterations         | $\gamma < 5\%$ | $\gamma < 10\%$ | $\gamma < 5\%$ | $\gamma < 10\%$ |
|                      | 7              | 6               | 7              | 6               |
| Time                 | 142 s          | 123 s           | 139 s          | 121 s           |

sphere ( $r_3 = 0.1$  m,  $\varepsilon_3 = 6$ ) as shown in Fig. 20. In this test case, we employ MoM in all sub-domains. The results from the original problem are compared to the full-wave solution using commercial software package FEKO. The total backscattered field on the  $x$ - $z$  plane is shown in Fig. 23 and in Fig. 24 for  $\gamma < 5\%$  and  $\gamma < 10\%$  respectively. The solid red line shows the fields calculated using the hybrid method, i.e., MoM-MoM-MoM. The dashed blue line shows the fields obtained from FEKO. We observe that

the hybrid method offers a good agreement with FEKO. Table 4 shows the performance of the hybrid method for this test case. As we can see, for the MoM-MoM-MoM combination, the generalized hybrid method converges after 35 iterations and 500 seconds for  $\gamma < 5\%$ , and 25 iterations and 365 seconds for  $\gamma < 10\%$ . The total number of unknowns is roughly 5.1 K. FEKO took 360 seconds to solve the same problem with the same total number of unknowns.

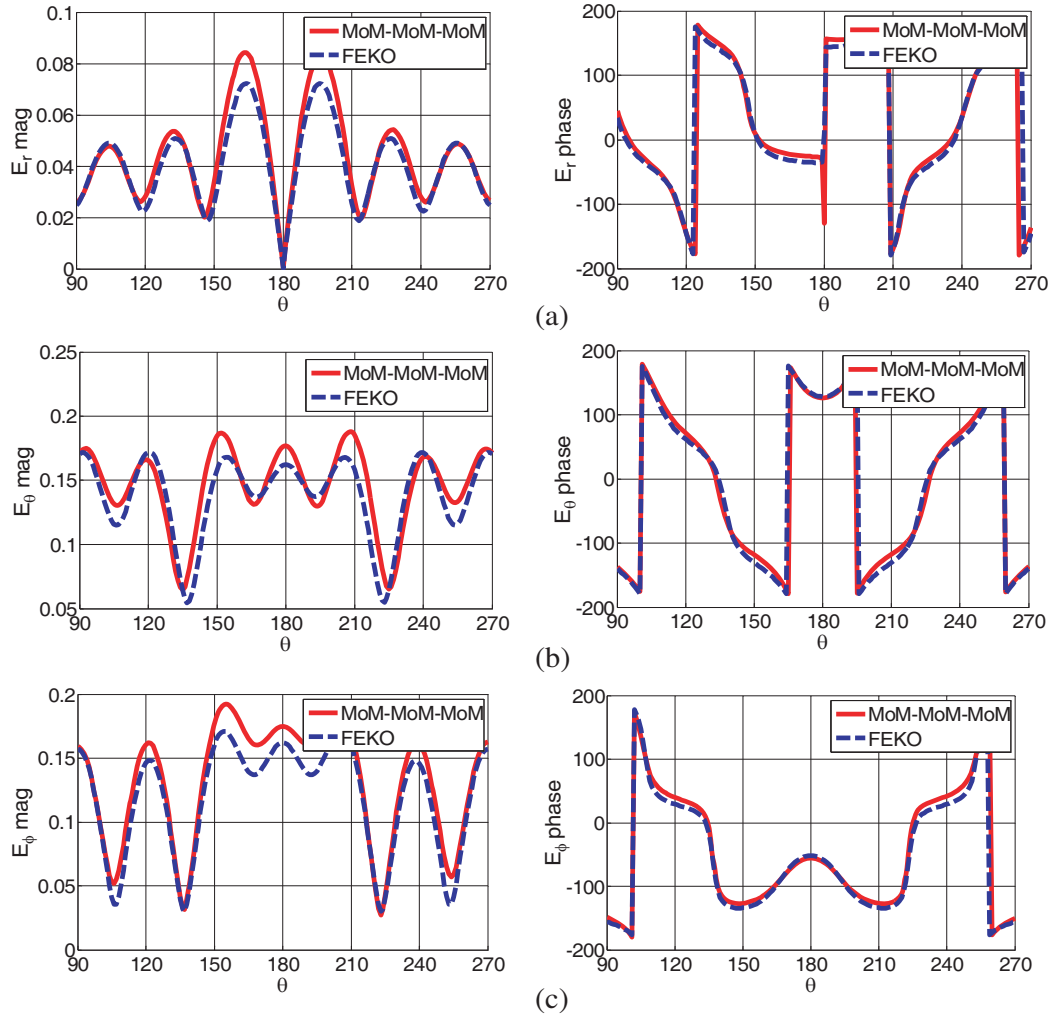


**Figure 23.** Backscattered field of a three-layered dielectric sphere at  $f = 1$  GHz using MoM-MoM-MoM for  $\gamma < 5\%$ . (a)  $E_r$  component magnitude and phase. (b)  $E_\theta$  component magnitude and phase. (c)  $E_\phi$  component magnitude and phase.

**Table 4.** Performance of the hybrid method for scenario 2, test case 2.

| Method               | MoM-MoM-MoM    |                 |
|----------------------|----------------|-----------------|
| # Unknowns (Maximum) | $\sim 2.2$ K   |                 |
| # Iterations         | $\gamma < 5\%$ | $\gamma < 10\%$ |
|                      | 35             | 25              |
| Time                 | 500 s          | 365 s           |

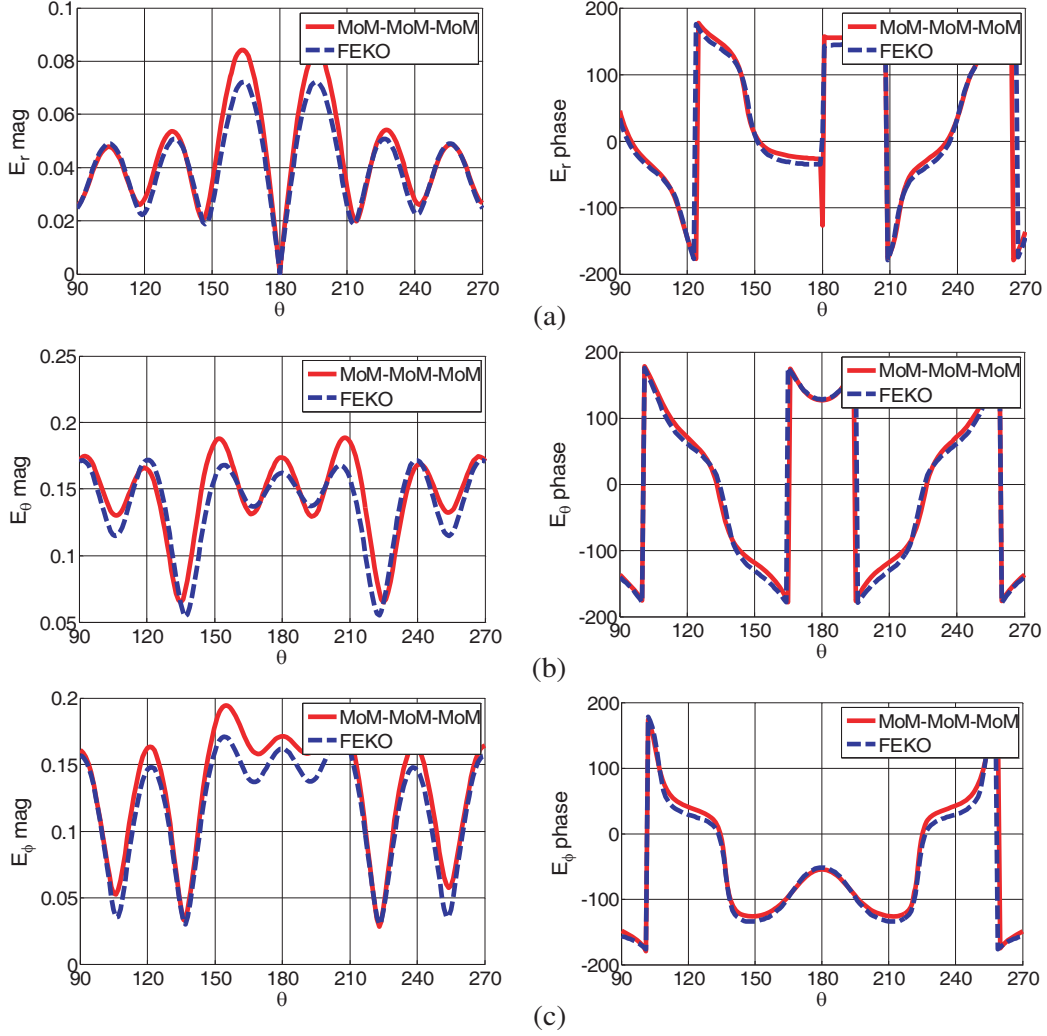


**Figure 24.** Backscattered field of a three-layered dielectric sphere at  $f = 1$  GHz using MoM-MoM-MoM for  $\gamma < 10\%$ . (a)  $E_r$  component magnitude and phase. (b)  $E_\theta$  component magnitude and phase. (c)  $E_\phi$  component magnitude and phase.

## 5. CONCLUSION AND FUTURE WORK

In this paper, a generalized hybrid method is proposed to solve electromagnetic scattering problems in two different scenarios: (i) multiple non-touching homogeneous objects, and (ii) inhomogeneous objects. This is achieved by dividing the original problem into separate sub-domains. The solution for the entire domain is found by using either an analytical or numerical approach as appropriate for each sub-domain, followed by an iterative procedure between the sub-domains. The generalized hybrid method shows a good agreement in terms of accuracy with the commercial software package, FEKO. In this paper, we have limited our analysis to isotropic scatterers. More complex geometries, including anisotropic scatterers and scatterers with cavities, will be considered in the future. Furthermore, the parallel implementation details of the generalized hybrid method will also be addressed in the future.

## REFERENCES

1. Harrington, R. F., *Field Computation by Moment Method*, Krieger Publ., Malabar, FL, 1982.

2. Yee, K. S., "Numerical solution of initial boundary value problems involving Maxwell's equations in isotropic media," *IEEE Trans. Ant. Propag.*, Vol. 14, 302–307, 1966.
3. Jin, J. M., *The Finite Element Method in Electromagnetics*, John Wiley & Sons, New York, 1993.
4. Volakis, J. L., A. Chatterjee, and L. C. Kempel, *Finite Element Method for Electromagnetics: Antennas, Microwave Circuits, and Scattering Applications*, IEEE Press, Piscataway, New Jersey, 1998.
5. Coifman, R., V. Rokhlin, and S. Wandzura, "The fast multipole method for the wave equation: A pedestrian prescription," *IEEE Antennas Propagat. Mag.*, Vol. 35, No. 3, 7–12, Jun. 1993.
6. Song, J. M. and W. C. Chew, "Multilevel fast multipole algorithm for solving combined field integral equations of electromagnetic scattering," *Microw. Opt. Tech. Lett.*, Vol. 10, 14–19, Sep. 1995.
7. Canning, F. X., "The impedance matrix localization (IML) method for moment-method calculations," *IEEE Antennas Propagat. Mag.*, Vol. 32, No. 5, 18–30, 1990.
8. Bleszynski, E., M. Bleszynski, and T. Jaroszewicz, "AIM: Adaptive integral method for solving large-scale electromagnetic scattering and radiation problems," *Radio Science*, Vol. 31, No. 5, 1225–1251, 1996.
9. Stupfel, B. and M. Mognot, "A domain decomposition method for the vector wave equation," *IEEE Trans. Antennas Propag.*, Vol. 48, No. 5, 653–660, May 2000.
10. Li, Y.-J. and J.-M. Jin, "A new dual-primal domain decomposition approach for finite element simulation of 3-D large-scale electromagnetic problems," *IEEE Trans. Antennas Propag.*, Vol. 55, No. 10, 2803–2810, Oct. 2007.
11. Lu, C. C. and W. C. Chew, "The use of Huygens' equivalence principle for solving 3-D volume integral equation of scattering," *IEEE Trans. Antennas Propag.*, Vol. 43, No. 5, 500–507, May 1995.
12. Jensen, M. A. and J. D. Freeze, "A recursive Green's function method for boundary integral analysis of inhomogeneous domains," *IEEE Trans. Antennas Propag.*, Vol. 46, No. 12, 1810–1816, Dec. 1998.
13. Xu, F. and W. Hong, "Analysis of two dimensions sparse multicylinder scattering problem using DD-FDTD method," *IEEE Trans. Antennas Propag.*, Vol. 52, No. 10, 2612–2617, Oct. 2004.
14. Monorchio, A., A. R. Bretones, R. Mittra, G. Manara, and R. G. Martin, "A hybrid time-domain technique that combines the finite element, finite difference and method of moment techniques to solve complex electromagnetic problems," *IEEE Trans. Antennas Propag.*, Vol. 52, 2666–2673, 2004.
15. Al Sharkawy, M. H., V. Demir, and A. Z. Elsherbeni, "The iterative multi-region algorithm using a hybrid finite difference frequency domain and method of moment techniques," *Progress In Electromagnetics Research*, Vol. 57, 19–32, 2006.
16. Hodges, R. E. and Y. Rahmat-Samii, "An iterative current-based hybrid method for complex structures," *IEEE Trans. Antennas Propag.*, Vol. 45, No. 2, 265–276, 1997.
17. Jakobus, U. and F. M. Landstorfer, "Improved PO-MM hybrid formulation for scattering from three-dimensional perfectly conducting bodies of arbitrary shape," *IEEE Trans. Antennas Propag.*, Vol. 43, No. 2, 162–169, 1995.
18. Chen, M., X. W. Zhao, Y. Zhang, and C. H. Liang, "Analysis of antenna around NURBS surface with iterative MoM-PO technique," *Journal of Electromagnetic Waves and Applications*, Vol. 20, No. 12, 1667–1680, 2006.
19. Carr, M. and J. L. Volakis, "Domain decomposition by iterative field bouncing," *IEEE AP-S International Symposium (Digest)*, Vol. 3, 298–301, San Antonio, TX, 2001.
20. Kim, C. S. and Y. Rahmat-Samii, "Low profile antenna study using the physical optics hybrid method (POHM)," *Antennas and Propagation Society International Symposium, 1991, AP-S Digest*, 1350–1353, IEEE, 1991.
21. Nguyen, Q. and O. Kilic, "Electromagnetic scattering from multiple domains using a hybrid numerical and analytical solution," *ACES 2014*, Jacksonville, FL, USA, Mar. 23–27, 2014.
22. Nguyen, Q. and O. Kilic, "A hybrid method for electromagnetic scattering from multiple conducting objects," *APS-URSI 2014*, Memphis, TN, USA, Jul. 6–12, 2014.

23. Phan, T., Q. Nguyen, and O. Kilic, "A hybrid technique for electromagnetic scattering from three-dimensional inhomogeneous dielectric objects," *ACES 2016*, Honolulu, Hawaii, Mar. 13–17, 2016.
24. Hansen, J. E., et al., *Spherical Near-Field Antenna Measurements*, Vol. 26, ser. IEE Electromagnetic Waves Series, Peter Peregrinus, London, UK, 1988.
25. Devaney, A. J. and E. Wolf, "Multipole expansions and plane wave representations of the electromagnetic field," *Journal of Mathematical Physics*, Vol. 15, No. 2, 234–244, 1974.
26. Cappellin, C., O. Breinbjerg, and A. Frandsen, "Properties of the transformation from the spherical wave expansion to the plane wave expansion," *Radio Sci.*, Vol. 43, No. 1, 2008.
27. Atkinson, C. K., "Numerical integration on the sphere," *J. Austral. Mat. Soc. B*, Vol. 23, No. 3, 332–347, 1982.
28. Abramowitz, M. and I. A. Stegun, *Handbook of Mathematical Tables*, Dover, 1970.
29. Nguyen, Q. and O. Kilic, "An alternative plane wave decomposition of electromagnetic fields using the spherical wave expansion technique," *IEEE Antennas and Wireless Propagation Letters*, Vol. 16, 153–156, 2017.